Proceedings of ASME 2024
International Symposium on Flexible Automation
ISFA2024
July 21-24, 2024, Seattle, WA

ISFA2024-141314

DIGITAL FRINGE PROJECTION FOR INTERLAYER PRINT DEFECT CHARACTERIZATION IN DIRECTED ENERGY DEPOSITION

Guanzhong Hu[1], Rujing Zha[1], Yaoke Wang[1], Jian Cao[1], Ping Guo[1]

[1]Department of Mechanical Engineering, Northwestern University, Evanston, IL

ABSTRACT

Directed Energy Deposition (DED) is one of the main additive manufacturing (AM) families, enabling the fabrication of multi-material parts with high material addition rates. However, the incremental nature of DED fabrication makes it prone to local defect formation due to process condition fluctuations. Known for its rapid and precise 3D surface measurement capabilities, digital fringe projection (DFP) was previously demonstrated in process monitoring for powder bed AM. This study brings DFP to the DED process through development of a custom motor stage system and validates its effectiveness in assessing surface topography and build height measurement. Measurements were taken on both correctly deposited builds and builds with off-nominal deposition conditions, where the system was able to detect pitting as small as 0.425 mm in the lateral size and 0.154 mm in depth in the case of reduced laser energy. This work paves the way for future machine learning-enabled interlayer defect identification, classification, and healing via altering subsequent processing settings.

Keywords: digital fringe projection; directed energy deposition; non-coherent imaging; surface topography

1. INTRODUCTION

Laser powder-blown directed energy deposition (DED) is a flexible additive manufacturing (AM) process in which powder feedstocks flow into a laser-formed molten pool, forming beads that stack layer-by-layer to form a printed part. DED has significant potential to disrupt manufacturing with its ability to fabricate highly optimized geometries with continuously varied compositions and microstructures. DED, like other additive techniques, can suffer from many types of defects, such as lack of fusion porosity and geometric inaccuracy due to the local nature of the deposition process which merges many different physics. There is therefore a need to detect manufacturing defects in DED as they occur.

Many in-situ geometric monitoring techniques have been investigated to identify defect-forming regions and implement correction strategies. For instance, Fathi et al. used a CCD camera to detect the side profile of a DED build and used this as input to control the build height by varying the deposition speed [1]. However, this measurement strategy can only provide two-dimensional silhouettes and does not directly capture the entire profile of a three-dimensional part. More recently, Chen et al. [2] used a laser line scanner to identify defects in the surface profile in laser directed energy deposition. However, the nature of the line scanner left regions of missing data in the direction transverse to the line direction. While this could conceivably be resolved via slower scanning or rescanning at different angles, these strategies add complexity to the measurement system and are unsuitable for in-process measurement.

One potential technique for DED involves interferometric methods, such as shadow or projection moiré [3]; however, their implementation requirements make them a poor fit for additive applications. Digital fringe projection (DFP) provides a low-cost, high-resolution alternative to traditional interferometry techniques, requiring only a standard monochrome camera and a projector system with relatively relaxed resolution requirements for highly sensitive out-of-plane measurements. Though the technology relies on the same principle as interferometry – namely, extracting a field of phases from distorted fringes – fringe projection works via directly projecting the fringes, rather than interfering two grating patterns. The DFP technology is relatively mature and has been applied to laser powder bed fusion [4]; however, the technique's ability to detect defects has not yet been studied in detail for DED. The proposed method utilizes DFP's full-field, high-speed, and high-precision measurement

capabilities to comprehensively monitor the DED manufacturing process.

A monitoring system using DFP has the potential to achieve in-process metrology and closed-loop control of the process in DED manufacturing. As shown in Fig. 1, following the completion of each new layer by the DED deposition, the **A** stage rotates to present the part to the DFP system. Upon detecting any anomalies, based on the DFP measurement results, control strategies can correct the defects during the process in subsequent printing. In addition, geometric compensation can be applied during the print by monitoring the thermal distortion of the printed parts. The proposed DFP system can therefore provide invaluable part geometric data, which analytical or machine learning algorithms may then use to determine geometric accuracy and identify defect probability.

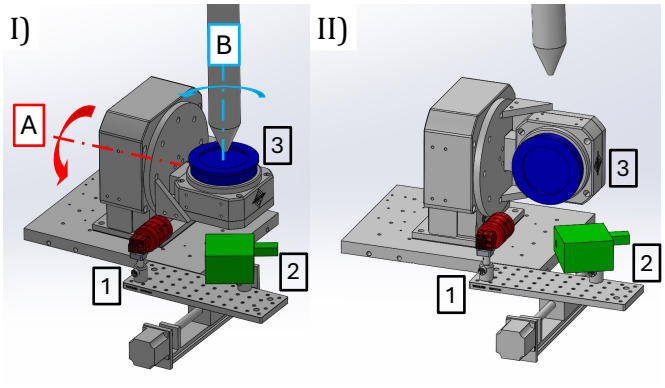

FIGURE 1: CONCEPTUAL SETUP OF THE DIGITAL FRINGE PROJECTION SYSTEM IN DIRECTED ENERGY DEPOSITION MACHINE: I) PRINTING MODE AND II) MEASUREMENT MODE. (1) CAMERA (2) PROJECTOR (3) SUBSTRATE AND PRINTED PART.

The focus of the study is on adjusting and optimizing the DFP system to effectively detect and quantify potential build defects in the DED process. This research constructs a platform integrating DFP into the DED environment, accounting for the differing geometric requirements of DED compared to powder bed based AM methods.

This paper is outlined as follows. First, the calibration method for DFP systems in DED is introduced, including calibration of pixel size and phase to vertical measurement. Next, the surface morphology of multiple DED-printed parts is successfully reconstructed and compared to the results generated from a 3D scan generated using focus-variation metrology. Finally, this method is applied to two case studies to qualitatively identify the defects induced by inappropriate process parameters in DED, such as the effects of laser power and powder flow rate on printing. Through this research, DFP is found to serve as a feasible technology for process inspection and measurement in DED and a viable data stream for closed-loop control of DED process parameters.

2. MATERIALS AND METHODS

2.1 Hardware development

A set of DFP equipment from *Phase3D Inc*. was utilized for fringe projection and image processing. The hardware includes an Allied Vision Alvium 1800 U-1242m camera (resolution of 4128 × 3008 pixels) equipped with an Edmund Optics HP Series fixed focal length lens (f = 50 mm). A Keynote Photonics LC3010-RGB10/OF projector (resolution of 1280 × 720 pixels), which has adjustable focus, was controlled by the Phase3D software to project the fringes.

The DFP setup was mounted on a stepper motor-driven ball screw linear actuator (FUYU FSK40F200-10C7). The platform is capable of translational movement with positioning accuracy of 50 microns. Given the build plane is moved upwards during each layer of printing in DED, this movable platform enables the printed object's surface to always remain within the camera's depth of field. More importantly, it maintains the distance between the camera and the top surface of the printed object, ensuring consistency of the calibration parameters. The linear actuator was controlled by an Arduino Uno Rev3, which also triggers the camera and projector to synchronize their operations. The data itself is registered and processed on a Windows 11 computer.

To facilitate the convenient analysis of the DFP system and ensure its proper functioning within real DED machines, an experimental setup was constructed based on the internal space within the DED machine consisting of two manual linear stages on an optical breadboard. This setup provided a one-to-one analogue of the spatial relationship between the DFP system and the objects being measured in the DED system targeted for integration. In the targeted platform for implementation, the substrate is placed on a two-axis rotary stage, as shown in fig. 1. The **A** stage rotates the specimen between the vertical deposition system and the horizontal measurement system, while the **B** stage enables the DFP system to measure different parts on the same build plate. All components of the DFP system were integrated onto an aluminum base to maintain the critical angles

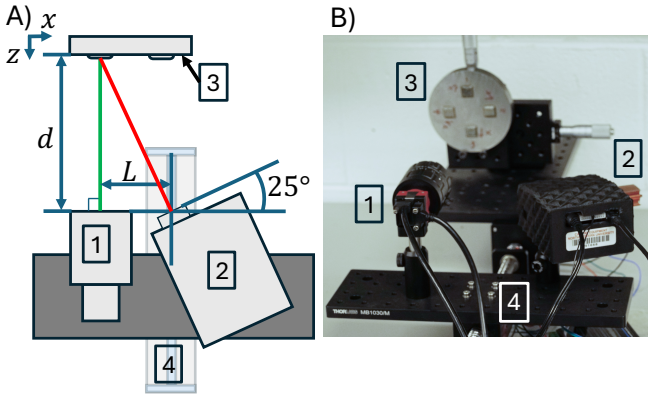

FIGURE 2: A) SCHEMATIC OF DIGITAL FRINGE PROJECTION SYSTEM; B) DIGITAL FRINGE PROJECTION SYSTEM SETUP. (1) CAMERA (2) PROJECTOR (3) REFERENCE SURFACE (4) LINEAR ACTUATOR.

and distances between the part under investigation and the sensing equipment. The whole in-situ detection system, consisting of a camera, projector, linear actuator, and aluminum base, measures 410 × 310 × 220 mm and can be quickly installed and removed within a closed printing chamber in the future, without occupying excessive space.

Fig. 2 illustrates the placement of components in the system. The projection direction always forms a 25-degree angle with the normal vector of the reference plane (*z*-axis). The camera faces the reference surface, with an observation distance d between the lens and the reference surface of 200 mm. The camera lens and the projection lens are aligned with respect to the *z*-axis, and the distance between them on the direction of the *x*-axis, *L,* is 120 mm. Due to the irregular texture of the metal print, the reflective surface after melting, and the flat metal substrate, some areas still show specular reflection, leading to saturation in the image [5].

Due to the adverse effects of ambient light on the accuracy of DFP measurements [6], the entire experiment was conducted in a stable ambient light environment. The observation window of the Additive Rapid Prototyping Instrument (ARPI), an open-architecture laser-powder DED instrument at Northwestern University, is equipped with a laser safety window (Kentek ACRX-BB2) to protect operators from the bright melt pool radiation and scattered laser light. These features also contribute to reducing the intensity of light within the machine, providing a suitable operation environment for the DFP system within the DED machine in the future.

2.2 Principle of digital fringe projection

DFP is a method that a regular sinusoidal fringe onto the surface of the object being measured, and then observes and records the distortion of the fringe on the object by estimating the local phase of the fringes' intensity to measure the morphology of the object surface [7,8]. The patterns' irradiance distribution of these patterns is expressed as:

$$I_i(x) = I_0\left[cos\left(\frac{2\pi x}{P} + \delta_i\right) + 1\right] \tag{1}$$

where I_i indicates the i^{th} frame, I_0 is the irradiance modulation, x is the location along the object where the measurement is taken, and P is number of pixels per fringe period, also known as fringe pitch. The step size of the projected fringe will be determined based on the number of shots N for each instance. δ_i is the time-varying phase shift which is given by

$$\delta_i = \frac{i-1}{N}2\pi, i = 1, \dots, N \tag{2}$$

After the camera records the pattern from the object, a wrapped phase map is obtained by applying the phase-shifting algorithm. The wrapped phase can be represented by the following equation:

$$\phi(x) = \arctan\left(\frac{-\sum_{i=1}^{N} I_i(x)\sin\delta_i}{\sum_{i=1}^{N} I_i(x)\cos\delta_i}\right) \tag{3}$$

Thus, the phase offset ϕ is obtained. By subtracting the phase offset with respect to the reference plane with the object x_0 from the phase offset with respect to the empty reference plane x_r, the object-reference point's phase difference is given from [8] as:

$$\phi = \phi_o - \phi_r = \frac{2\pi(x_o - x_r)}{P} \tag{4}$$

This phase difference directly correlates to the differential measurement height. The height measurement can be obtained by multiplying the phase differences by a calibrated constant detailed in Section 2.3.

Assuming that the distance L between the projector and the camera is much greater than the geometric distance between x_0 (phase offset at object position) and x_r (phase offset at the empty reference plane) [8]. The measurement in this experiment conforms to this assumption. The height z of the measurement point from the reference plane can be expressed as:

$$z = \frac{d(x_0 - x_r)}{L} \tag{5}$$

The relationship between the phase difference and the height of the measurement point relative to the reference plane can be obtained through Equations (4) and (5):

$$z(\phi) = \frac{Pd\phi}{2\pi L} \tag{6}$$

Due to hardware limitations, precise positions of the camera sensor and projection light source cannot be obtained. Additionally, since DED always uses the method of upward stacking to construct objects, parameters such as the fringe pitch P and observation distance d cannot be precisely determined using analytical methods for a static hardware configuration. Furthermore, the observation distance d constantly change while printing each new layer, complicating the measurement process further. By using a linear actuator to move the DFP system, the relative positions between different reference surfaces, cameras, and projections remain consistent, simplifying the need for recalibration in different positions. Since these variables remain constant during the measurement process, they can be replaced by a calibrated constant C:

$$C = \frac{Pd}{2\pi L} \tag{7}$$

2.3 DFP calibration

To obtain the height map and surface normal map of the DED printed parts, a calibrated constant to construct the height map from the phase map is required. The calibration of the DFP

system includes two steps. First, it is necessary to measure the pixel size of the camera to obtain the cross-sectional area of the object. Standard gauge blocks were used to measure pixel dimensions. A rectangular gauge block was placed on the reference plane, and the linear actuator in Fig. 2 was used to move the camera backward so that the distance from the surface of the gauge block to the lens was maintained at 200 mm. The pixel size can be calculated by measuring the size of the camera's field of view and the number of pixels the block occupies in the frame. The camera's field of view was found to be 49 × 36 mm, and the size of each pixel is 12 × 12 µm.

To obtain the true height corresponding to the phase difference, a 1-degree angle block was used to calibrate the DFP system. By extracting a section on the horizontal plane of the angle block, the height change of the angle block is known based on the set angle. It is used to fit the measured phase difference by least squares fitting to a straight line. The differential height then can be calculated for DFP based on the slope of the fitted line, the calibrated constant C, which is 1.06. By the measurement results of phase difference and height difference shown in Fig. 3, the object's height information can now be obtained from DFP.

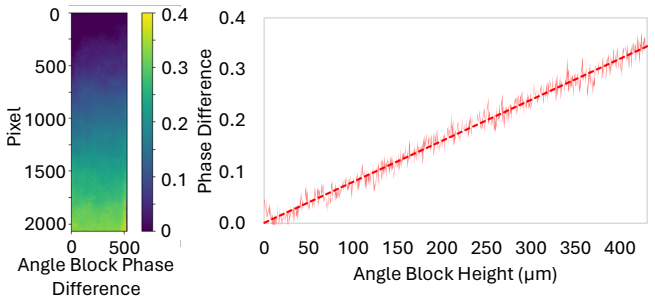

FIGURE 3: ANGLE BLOCK PHASE DIFFERENCE, AND THE ACTUAL HEIGHT CORRESPONDING TO THE PHASE DIFFERENCE.

The images were filtered with a low-pass filter implemented by transforming the image into the frequency domain via 2D fast Fourier transform and excluding high-frequency components of the signal. Based on this filtered data, the surface normal map of the measurement area was calculated based on the height map to illustrate the local surface texture variations.

2.4 Experimental design

In this experiment study, the object's overall height and surface relative height were measured using DFP to validate the morphology measurement. The height difference measurement capability of DFP is related to the fringe pitch P, where wider fringes can measure larger height differences, but with reduced sensitivity to capturing small height differences [9]. This experiment employed 3 mm fringe pitches to measure the object's overall height (relative to the substrate) and surface relative height (relative to the lowest point of the latest layer).

The experimental samples were fabricated using the ARPI system at Northwestern. The system comprises of a 1000-watt λ=1070 nm laser (IPG YLR-1000) coupled with Aerotech linear stages, a Precitec optics column, and a Fraunhofer COAX8 nozzle. A PowderMotionLabs X2 hopper system metered powder, which was blown onto the deposition location using Argon shielding gas (99.999% purity, 1 ppb O_2). The substrate used was a 15.8 mm thick 1018 low-carbon steel disc (McMaster-Carr #7786T52), while the feedstock was MetcoClad 316L-Si stainless steel powder (Oerlikon Metco, #1079454), with a particle size range of 45-106 µm. Table 1 shows the nominal and designed defective printing parameters of DED printing samples:

TABLE 1: PRINTING PARAMETERS OF DED SAMPLES

Printing parameters	Nominal value	Designed defect
Laser power (W)	600	300 (B3, B4)
$\frac{1}{e^2}$ laser diameter (mm)	2.22	
Powder feed (g/min)	14	7 (B1, B2)
Scan speed (mm/s)	7	
Hatch spacing (mm)	0.8	
Interlayer step (mm)	0.55	

This study aims to validate the effectiveness of DFP in detecting the overall height, relative surface height, and ability to identify printing defects in DED printed objects. The experimental design is schematically shown in Fig. 4. Two sets of samples (labeled as A and B) were printed using DED, each consisting of four rectangular blocks (labeled as 1 to 4) with different heights. The scanning strategy used for all experiments comprised a 12 mm square inside which bilinearly scanned hatches were deposited. Both the exterior square and the internal hatches rotated their starting location and direction by 90° every layer. In between each of the four layers, deposition was paused for 15 seconds in addition to the time taken to travel from the end of the last layer to the start of the next layer at the fast move speed of 20 mm/s. Table 1 details the nominal parameters (NOM) used for DED printing.

In the first set of samples, each block was printed with one, two, three, and four layers according to the nominal parameters

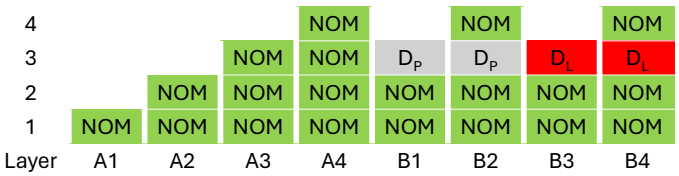

FIGURE 4: SCHEMATIC DIAGRAM OF LAYER PARAMETERS FOR THE NORMAL SAMPLES (A1-A4) AND DEFECTIVE SAMPLES (B1-B4) INDICATING LAYERS WITH NORMINAL (NOM), POWDER DEFECT, (D_P), AND LASER DEFECT (D_L) PRINT PARAMETERS.

as listed in Table 1, labeled as A1, A2, A3, and A4, respectively. In the second set of samples, each block was first printed with the first two layers using the nominal parameters, labeled as B1,

B2, B3, and B4. Then, there was a slight variation in the printing process for the third layer. To simulate a powder delivery defect (D_P), the powder delivery speed for B1 and B2 was reduced by 50% (7 g/mm) during the printing of the third layer. Similarly, to simulate a laser defect (D_L), the laser power for B3 and B4 was reduced by 50% (300 W) during the printing of the third layer. Finally, the fourth layer was printed with standard parameters on blocks B2 and B4.

After the two sets of samples were printed, they were removed from the print area. Any powder particles suspended on the surface of the samples were removed with high-speed airflow and tape. Then, the samples were placed in the rotating bracket for DFP measurements. Each sample was also scanned via focus-variation metrology on an Alicona InfiniteFocus G4 system.

3. RESULTS AND DISCUSSION

In this section, the accuracy of DFP measurements is validated by comparing by DFP with results from focus-variation microscopy. Additionally, the morphology detection capability of DFP will be verified by comparing the detected changes in the shape of printed objects with results induced by non-standard parameters.

3.1 Height measurement

Figure 5 illustrates the profile height curves of four nominal blocks, with the *x*-axis oriented perpendicular to the scanning direction of the topmost layer, as obtained from DFP and focus-variation metrology. It can be observed from the figure that two curves coincide in height, demonstrating that DFP can clearly capture the surface features of DED-printed objects. In the central region of the contour plots, a length of 10 millimeters was selected to compare the errors between the two measurement

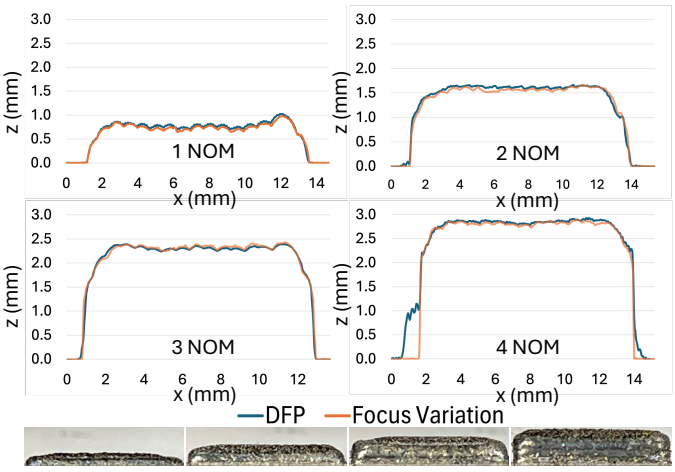

FIGURE 5: PROFILE OF NOMINAL DED PRINTED BLOCKS WITH 1, 2, 3, AND 4 LAYERS THICKNESS (A1–A4).

results. The errors for layers 1 through 4 were 5.8%, 3%, 0.7%, and 1.2%, respectively.

Compared to the shorter printing blocks, a significant error in height is observed on the left side of the base of the 4-layer printing block. This error is caused by occlusion of the projection system by the taller printed object. However, this error does not affect the overall height measurement or extracted surface feature information of the objects.

Measurements obtained through DFP indicate that the incremental height of each layer gradually decreases as the number of layers increases as shown in Fig. 5. This is due to an overbuilding condition in this particular parameter set, where the layer height of the build is naturally greater than the *z*-increment of the deposition head, causing the layer height to passively approach the z-increment over time [10]. Due to factors such as

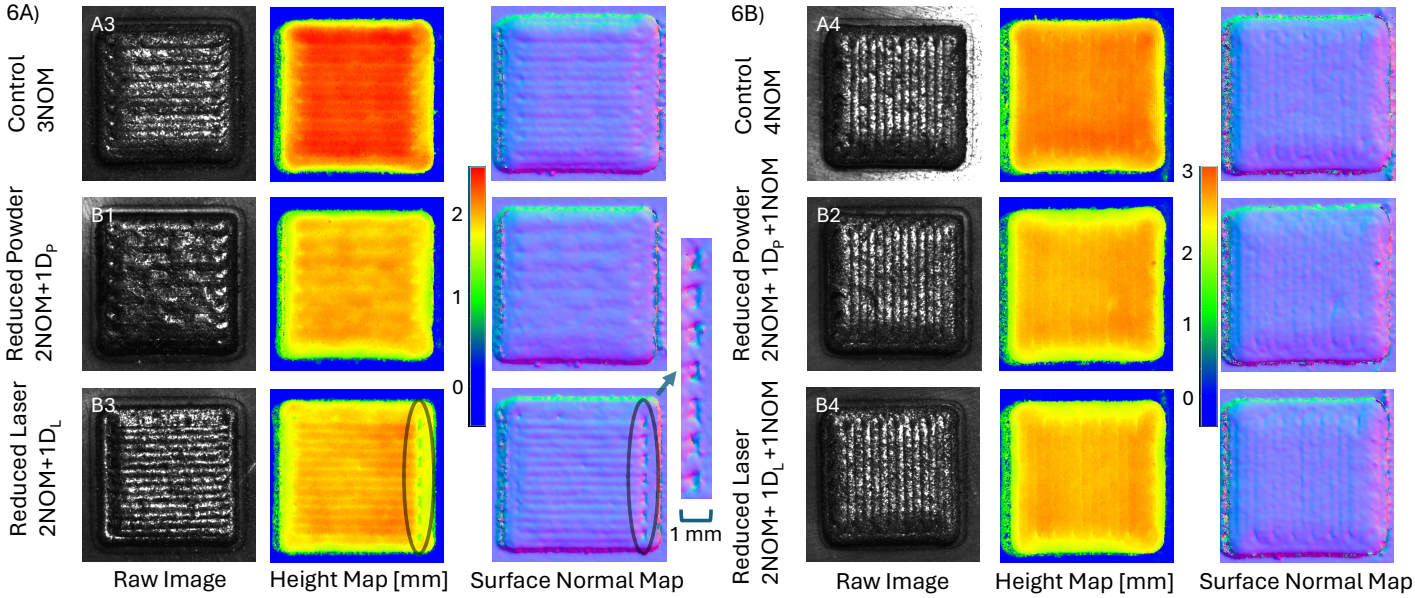

FIGURE 6: HEIGHTMAP AND SURFACE NORMAL MAP OF THE SAMPLE BLOCK. A) THREE THREE-LAYER BLOCKS A3, B1 AND B3; B) THREE FOUR-LAYER BLOCKS A4, B2 AND B4.

powder flow distribution, changes in working distance, and thermal accumulation effects, some powder may not be captured by the melt pool and instead falls onto the substrate. The ability of the phase projection system to capture the working height stability effect demonstrates its potential as a control signal input; for a given powder linear density, as the delta-z increment increases and powder efficiency improves, the deposition height can become unstable, resulting in a sinusoidal layer height defect [11]. Interlayer build height measurement via this technique may be used to identify zones with reduced height and deposit more material in those regions. Reducing overbuilding by increasing the delta-z increment into regions that are unstable in open-loop processing can improve the material consumption efficiency, reducing costs and supply chain risks.

3.2 Defect identification

Figures 6(a) and 6(b) demonstrate the measurement results of the captured images, overall height maps, and surface normal maps of three-layer and four-layer prints respectively. The vector of the surface normal is linearly mapped to RGB images as shown in the figure. Compared to the nominal parameter print of three-layer block A3, blocks B1 and B3, also consisting of three layers, had their powder feed rate and laser power, respectively, reduced by 50% each during the printing of the third layer. Blocks B2 and B4 have an additional fourth layer printed at the nominal deposition conditions.

When the powder feed rate is halved, the overlap region between each printing path reduces, reducing the frequency of the deposition track overlapping lines visible in B1. This phenomenon can be clearly observed from the surface normal maps of A3 and B1 shown in Fig. 6(a). The increased spacing between adjacent tracks can cause the formation of large columnar grains that grow across multiple layers, as these grains grow primarily at the edges of the melt pool [12,13]. These microstructures can lead to off-nominal anisotropy and a reduction in strength of the final part.

In the case of reduced laser power, the change of spatial frequency of the overlapping clads is less apparent compared to the reduced powder case. However, in the absolute height plot, there are seven clear pits visible to the right of the block between the outside contour and the internal hatches. From the fucus variation microscopy results, these pits exhibit widths ranging from 0.425 mm to 0.896 mm and depths from 0.154 mm to 0.441 mm. These pits are potential regions where lack-of fusion defects could occur, which would negatively affect part performance. These divots are also apparent on the left-hand side of the reduced powder feed rate case.

In either of these two cases, it is critical that the human operator —or online control algorithm—is notified immediately. As visible in Fig. 6(b), as the subsequent 4th layer prints, the defect becomes less visible once printing resumes at the correct deposition conditions. Due to the local nature of DED fabrication, however, the later nominally printed layers may not correct the previous defectively printed layers. This is because at low dilutions, the melt pool of subsequent layers may not completely fill the dent, causing lack-of-fusion pores to form. Even if the defective layers have a lower height than correctly printed layers, the build height stability effect tends to correct for these minor changes and serves to obscure defective deposition. The deposition process thus fails silently. In the case of lack-of-fusion defects, the problems may only be discovered in post-fabrication ultrasonic or XCT analysis, substantially wasting time and effort as the part must be completed before inspection. Worse, local microstructural defects may not be discovered at all, even if witness coupons are printed simultaneously.

As the DFP metrology technique can be directly implemented into a DED system to measure the interlayer part geometry, an operator or control algorithm may be alerted. Depending on the severity of the defect, the part may then be reworked in situ or the build may be canceled and restarted, thus saving machine and operator time.

4. CONCLUSION

This article introduces the application of DFP in DED. Through hardware development, including a custom-designed movable platform and synchronized camera projector system, the functionality of DFP enables high-precision interlayer evaluation of DED build geometry capable of resolving individual build tracks. Experimental results demonstrated DFP's ability to measure object height and evaluate print defects. This lays the groundwork for future realization of in situ monitoring and control of DED. Compared to existing DED detection methods, the novelty of DFP lies in its ability to directly capture the entire contour of three-dimensional parts from a single perspective. Its outstanding positional robustness improves detection efficiency while also reducing the space it occupies within the DED machine. With an outlook based on the current research findings, future work will focus on machine learning-enabled print defect identification based on the DFP measurements and in-situ rework of parts without operator intervention.

ACKNOWLEDGEMENTS

This research was supported by the National Science Foundation under grants CMMI-2216298 and DGE-2234667.

REFERENCES

[1] Fathi, A., Khajepour, A., Toyserkani, E., and Durali, M., 2007, "Clad Height Control in Laser Solid Freeform Fabrication Using a Feedforward PID Controller," Int J Adv Manuf Technol, **35**(3), pp. 280–292.

[2] Chen, L., Yao, X., Xu, P., Moon, S. K., and Bi, G., 2021, "Rapid Surface Defect Identification for Additive Manufacturing with In-Situ Point Cloud Processing and Machine Learning," Virtual and Physical Prototyping, **16**(1), pp. 50–67.

[3] Cloud, G., ed., 1995, "Geometrical Moire," *Optical Methods of Engineering Analysis*, Cambridge University Press, Cambridge, pp. 145–146.

[4] Zhang, H., Prasad Vallabh, C. K., and Zhao, X., 2023, "Machine Learning Enhanced High Dynamic Range Fringe Projection Profilometry for In-Situ Layer-Wise Surface

Topography Measurement during LPBF Additive Manufacturing," Precision Engineering, **84**, pp. 1–14.
[5] Lin, H., Gao, J., Mei, Q., He, Y., Liu, J., and Wang, X., 2016, "Adaptive Digital Fringe Projection Technique for High Dynamic Range Three-Dimensional Shape Measurement," Opt. Express, OE, **24**(7), pp. 7703–7718.
[6] Waddington, C., and Kofman, J., 2010, "Analysis of Measurement Sensitivity to Illuminance and Fringe-Pattern Gray Levels for Fringe-Pattern Projection Adaptive to Ambient Lighting," Optics and Lasers in Engineering, **48**(2), pp. 251–256.
[7] Zhang, S., 2018, *High-Speed 3D Imaging with Digital Fringe Projection Techniques*, CRC Press.
[8] O'Dowd, N. M., Wachtor, A. J., and Todd, M. D., 2021, "Effects of Digital Fringe Projection Operational Parameters on Detecting Powder Bed Defects in Additive Manufacturing," Additive Manufacturing, **48**, p. 102454.
[9] Zhang, B., Ziegert, J., Farahi, F., and Davies, A., 2016, "In Situ Surface Topography of Laser Powder Bed Fusion Using Fringe Projection," Additive Manufacturing, **12**, pp. 100–107.
[10] Haley, J. C., Zheng, B., Bertoli, U. S., Dupuy, A. D., Schoenung, J. M., and Lavernia, E. J., 2019, "Working Distance Passive Stability in Laser Directed Energy Deposition Additive Manufacturing," Materials & Design, **161**, pp. 86–94.
[11] Sammons, P. M., Gegel, M. L., Bristow, D. A., and Landers, R. G., 2019, "Repetitive Process Control of Additive Manufacturing With Application to Laser Metal Deposition," IEEE Transactions on Control Systems Technology, **27**(2), pp. 566–575.
[12] Xu, K., Li, B., and Jiang, C., 2023, "Adjusting Microstructure and Improving Mechanical Property of Additive Manufacturing 316L Based on Process Optimization," Materials Science and Engineering: A, **870**, p. 144824.
[13] Saboori, A., Gallo, D., Biamino, S., Fino, P., and Lombardi, M., 2017, "An Overview of Additive Manufacturing of Titanium Components by Directed Energy Deposition: Microstructure and Mechanical Properties," Applied Sciences, **7**(9), p. 883.